Scalable and efficient video coding using 3D modeling

Raphaèle Balter, Patrick Gioia, Luce Morin

Scalable and efficient video coding using 3D modeling

Raphaèle Balter[1,2], Patrick Gioia[1], and Luce Morin [2]

[1] FRANCE TELECOM R & D, 4 rue du Clos Courtel, 35512 Cesson-Sevigne, France
[2] IRISA-INRIA, Campus de Beaulieu, avenue du General Leclerc, 35042 Rennes, France

[1] ***Abstract*— In this paper we present a 3D model-based video coding scheme for streaming static scene video in a compact way but also enabling time and spatial scalability according to network or terminal capability and providing 3D functionalities. The proposed format is based on encoding the sequence of reconstructed models using second generation wavelets, and efficiently multiplexing the resulting geometric, topological, texture and camera motion binary representations. The wavelets decomposition can be adaptive in order to fit to images and scene contents. To ensure time scalability, this representation is based on a common connectivity for all 3D models, which also allows straightforward morphing between successive models ensuring visual continuity at no additional cost. The method proves to be better than previous methods for video encoding of static scenes, even better than state-of-the-art video coders such as H264 (also known as MPEG AVC). Another application of our approach is the fast transmission and real-time visualization of virtual environments obtained by video capture, for virtual or augmented reality, free walk-through in photo-realistic 3D environments, and numerous other image-based applications.**

***Index Terms*— 3D Model-based Coding, Second Generation Wavelets, 3D Reconstruction**

I. INTRODUCTION

With the development of video applications over networks and wireless devices such as cell phones and PDAs, low bit rate video compression is still a key issue. More precisely, distant visualization on heterogeneous terminals requires video coding schemes providing a scalable bitstream adaptable to multiple and variable terminal resources.

State-of-the art video coders rely on pixel-based prediction / correction paradigms and they provide very efficient compression algorithms for generic contents video sequences in a wide range of bitrates. Indeed, this type of compression scheme has been optimized to reach its best performances in the latest standard video coder H264 ITU/MPEG-AVC [1].

Exploiting particularities of the encoded content can dramatically improve compression efficiency by using specific coding schemes. Typically, 3D model-based video coding exploits the fact that the scene contains known objects for which a specific or generic 3D model is available and can be transmitted together with texture and animation parameters. This method produces very efficient compression and it is particularly well adapted to the video-conference field where a 3D model of the human face is used to represent the video sequence of the speaker [2]. However, it is necessary for the scene content to be known and that an *a priori* known 3D model is available both at the coder and the decoder [3]. For a video with unknown contents, 3D model-based coding may still be used if the scene is static, i.e. with no moving object inside, and acquired by a moving camera, by automatically reconstructing the captured 3D environment from the video and transmit it as a 3D model, a texture and camera parameters.

Automatic 3D modeling of static scenes from uncalibrated images and video sequences has been studied for a long time, using computer vision structure-from-motion and self-calibration techniques [4] [5] [6] [7]. Most previous work focused on off-line video analysis for obtaining an accurate 3D model of the scene in order to replace manual modelling or to provide a precise reference frame for augmented reality [8], but few works have considered the issues of compressing and streaming the resulting 3D representation.

Such considerations have been mainly addressed for transmitting synthetic 3D models. Several methods have been proposed for the efficient and scalable coding of the 3D models geometry and connectivity providing a progressive and scalable bitstream [9] [10] [11]. It is assumed that texture will be transmitted as an image using standard fixed image coders or as a few parameters in the case of parametric texture. However, in the case of 3D models extracted from videos, texture is the most expensive information to be transmitted, and it is also a major factor in the final visual quality. With such input data, an effective 3D model coding and streaming scheme should take into account the geometry, connectivity and texture. In the context of multi view-point acquisition, as studied in the MPEG-3DAV consortium [12], real-time streaming of 3D point-based representation has been proposed, assuming fixed and calibrated cameras [13]. Other approaches seek to compress image-based rendering view-sets of virtual environment [14]. 3D information can be used to compensate disparity between between images [15]. However all those representations are often limited to small objects or require a particular capture system.

In order to benefit from the compactness and from the functionalities of 3D model-based coding in the case of unknown scene contents and uncontrolled acquisition procedure, we propose a video coding scheme based on a set of successive 3D models extracted from sub-sections of the video, instead of a unique one containing all the information viewed in the

[1]Article submitted to IEEE Transactions on multimedia

entire video sequence, as in previous automatic shape-from-motion schemes [7]. This choice has several advantages:

- Global consistency of extracted 3D information is not required. This allows us to simplify estimation and use inaccurate camera parameters.
- The set of 3D models directly provides a streaming format.
- Global illumination changes along time are modeled and reconstructed.
- Sequences of arbitrary size can be processed with on-the-fly estimation and streaming of the 3D models.
- Camera motion is unconstrained as long as it is not degenerated (e.g a pure rotation) and as its amplitude is sufficient to allow self-calibration.

Our first experiments validated this approach for low bitrate coding [16]. This scheme still allows 3D functionalities usually provided by classical 3D model-based video coding, such as illumination changes, object insertion, stereoscopic visualization or virtual viewpoints generation [17].

However, the previously proposed scheme does not provide full scalability, which is a key point for targeted applications such as distant and interactive visualization. In particular, mesh geometry has fixed resolution. It involves, furthermore, a complex and computationally expensive morphing and re-meshing process at the decoder side to ensure smooth visual transition between successive 3D models [16][18].

In both image coding and synthetic 3D models coding, wavelets [19] have been effectively used to achieve scalability in an elegant and efficient way. Second generation wavelets [20] provide hierarchical representations for arbitrary sampled data and they are the current most effective tool for scalable representation of 3D models [21].

Therefore we propose a scalable video coding scheme based on wavelet decomposition of an *evolving model* represented by a consistent 3D models stream. It provides low bit rate coding as well as time and spatial scalability and 3D functionalities. Targeted applications include impact simulation, and help for geo-positioning or virtual tourism.

In the following study, we firstly give an overview of the proposed method, then we briefly describe the extraction of 3D models in section III and explain the proposed hierarchical representation more thoroughly in section IV. We then present inter-relations between media flows and we explain the coding and decoding schemes in section V. Finally the results on real video sequences are finally shown and discussed.

II. Overview of the method

The proposed representation is based on 3D information extracted with the Galpin reconstruction algorithm. For each subsection of the sequence called a *GOF (Group of Frames)* it provides a dense depth map and camera positions for each frame in the GOF. The behavior of the coder is then as follows.

The first step is to transform each depth map into a hierarchical 3D triangular mesh. We define the *base mesh* , denoted BM_k as the mesh related to GOF k at coarser level and the *fine mesh* , denoted FM_k as the dense mesh related to GOF k at finer level. The refinement from coarser to finer level is then expressed as wavelets coefficients ($r_i{}^j$ on Fig. 1) using a second generation wavelet transform. Scale coefficients ($e_i{}^j$ on Fig. 1) represent the geometry of the base mesh BM_j. Successive 3D models in the stream are encoded differentially with coefficients $d_i{}^j$.

To ensure time consistency of the wavelets coefficients for successive models, wavelet decomposition is applied based on a single connectivity mesh (SCM), possibly evolving in time, and gathering the connectivities of each base mesh model.

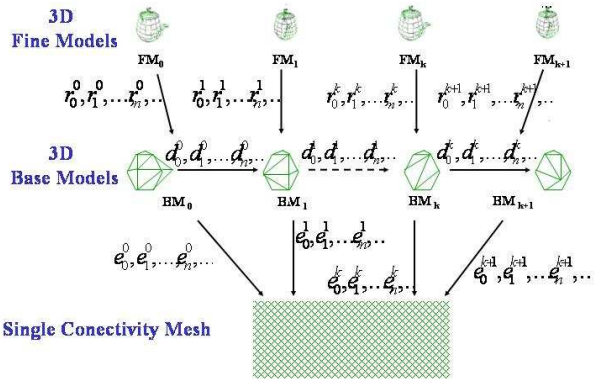

Fig. 1. Proposed representation based on a 3D model stream and second generation wavelets.

This representation induces several media streams, such as topology (the connectivity of the single base mesh), geometry (wavelet coefficients and incremental model representation), and texture. These streams are closely interrelated and they are multiplexed in order to produce a single streamable format.

In the following sections we describe the main components and the stream types they generate further.

III. 3D models generation

The 3D models stream is automatically extracted from the input video sequence using shape from motion methods developed in computer vision [5] . Each 3D model is extracted and used for a restricted portion of the video sequence called a GOF. Two successive GOFs share one image (cf. Fig. 2). These border images are usually called *keyframes*. Keyframes are automatically selected according to video contents, based on several criteria. These criteria mainly depend on motion, percentage of outgoing points in images and 3D reconstruction feasibility and stability [17]. On average a GOF contains 30 frames.

Disparity estimation is performed by a dense mesh-based affine motion estimator using multi-grid and multi-resolution approaches [22]. This robust algorithm minimizes the EQM and allows to estimate large disparities with lighting variations, thanks to mesh deformation. The motion field is then readjusted under epipolar geometry constraint. The camera intrinsic parameters are either estimated using self-calibration or set to approximate values. Extrinsic parameters define camera 3D motion during the acquisition. They are computed

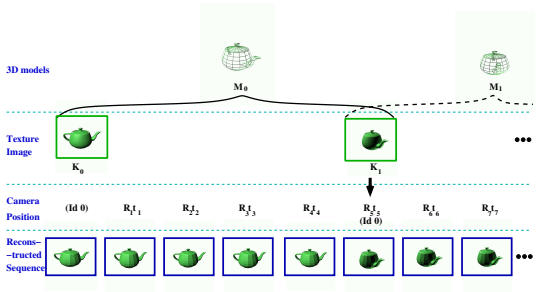

Fig. 2. Reconstruction of the original sequence

using classical self-calibration methods and an adapted bundle adjustment algorithm [17] allowing readjustment between models that is necessary for virtual reality applications. The dense motion field from the first to the last image of the GOF and camera parameters for these two images allow the reconstruction of a dense depth map for the first image of the GOF. Fig. 3 shows an example of such a depth map extracted from the *Street* video sequence. Camera extrinsic parameters are then retrieved for each image in the video sequence using a pose estimation algorithm.

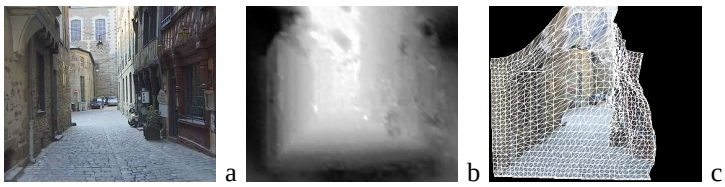

Fig. 3. An example of a depth map (b) extracted from the *Street* video sequence, the associated vrml model (c) and the corresponding image in the sequence (a).

The 3D reconstruction step thus provides for each GOF:

- the 3D model geometry: a dense depth map of the scene viewed from the first image in the GOF
- the 3D model texture: the first image in the GOF
- camera parameters for each frame in the GOF.

IV. Hierarchical 3D Models

We now explain how the hierarchical 3D triangular mesh is constructed from the dense depth map.

A. Notations

The following notations will be used in the rest of the paper:

- ${M_k}^i$ is the 3D model related to GOF k at resolution i
- K_k is the keyframe for GOF k (i.e. the first image in GOF k, also used as texture image T_k for ${M_k}^i$).
- C_k is the camera position related to keyframe K_k. C_k is defined by a translation t_{t_k} and a rotation R_{t_k}.
- CM_k is the corresponding mesh; it denotes the 3D model associated with GOF k whose vertices match vertices in the precedent model ${M^i}_{k-1}$ that are still visible from C_k and the related faces.
- We denote as $Pr(M, T, C)$ the image issued from perspective projection of 3D model M textured with image T onto the viewpoint related to camera C.

B. Single connectivity mesh and global indexing

Using a stream of 3D models instead of a unique one for the whole sequence provides several benefits that were mentioned previously. However, it also has the drawback of independently and arbitrarily sampling each 3D model. As a consequence, the vertices of two successive models are not matching points, whereas the models usually represent largely overlapping parts of the scene. Applying hierarchical wavelet decomposition on such independently sampled models leads to high residual information and sub-optimal coding efficiency. Moreover, such independent sampling prevents smooth swapping between 3D models at visualization stage. Therefore we propose to build a consistent sampling for all 3D models with vertices corresponding to identical physical points. This is done by separating connectivity and geometry; a planar graph, denoted as *single connectivity mesh (SCM)*, gathers the connectivity information of every base mesh in the sequence, regardless of their geometry. This mesh evolves during time in order to take into account outgoing and incoming points. The SCM is computed starting from the connectivity information of the first base mesh, and updated with the connectivity information associated with new points appearing from one base mesh to another. The SCM computation and update is based on the base meshes construction described in section IV-C. A global indexing system provides a unique index for each vertex in the SCM, thus implicitly defining matching between base meshes vertices. The SCM is described as a list of triangles expressed in the new global indexing system. The SCM also provide a unique index for each face in the SCM.

Wavelet decomposition based on the SCM is consistent for all models and leads to compact coding. Moreover, smooth swapping at visualization can then be achieved by direct morphing between vertices without ghost effect due to a fading [17] nor morphing additional computing cost [16] [18]. This can be done at each level of subdivision thanks to the consistent connectivity of all base meshes and the global index system. Indeed thanks to base mesh faces global index, a unique index can be computed for all vertices at each level using his barycentrical coordinates in base face. At each level i, smooth transition between models M_k and M_{k+1} can be achieved by linear interpolation between corresponding vertices:

$$M_c = \alpha * {M^i}_k + (1-\alpha) * {M^i}_{k+1} \text{ with } \alpha = \frac{\| t_{t_{k+1}} - t_{t_c} \|}{\| t_{t_{k+1}} - t_{t_k} \|},$$

where M_c denotes the interpolated model for current time t_c and t_{t_c}, t_{t_k} and $t_{t_{k+1}}$ denote translation vectors defining camera position for the current frame, keyframe K_k and K_{k+1} respectively.

C. Base meshes construction

Base meshes use non-uniform triangulation in order to ensure global connectivity consistency and smooth transition between models. Furthermore to better represent the video content, the base mesh must also to fit features of the scene.

For the first GOF, the adaptive triangular mesh is based on feature points computed on the first frame in the GOF

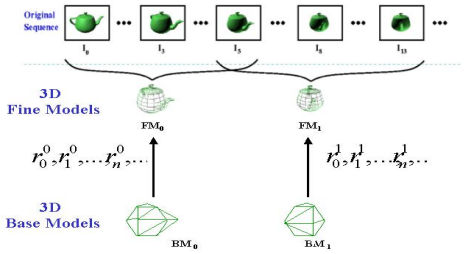

Fig. 4. Principle of the Wavelet Decomposition for the 3D Model Stream

(keyframe), using a block-based Harris corner detector [23]. The size of block used for Harris detection fixes the number of the base mesh vertices (e.g. 200 vertices for our experiments). A 2D Delaunay triangulation of these points under the constraint of image borders provides the base mesh connectivity. In order to avoid texture stretching near image borders, we add vertices on image borders. The 3D base mesh BM_0 is then derived by elevation of this 2D mesh using 3D information provided by the depth map.

In order to build the SCM, each base mesh is forced to contain the correspondents of the previous base mesh vertices, if they are still visible in the GOF. To meet the SCM constraint, triangles of these correspondents, whose set is denoted by CM_k, are included in the base mesh: $CM_k \subseteq BM_k$.

When adding vertices on the border of the model, the new triangulation has to preserve the connectivity derived from the preceding GOF without edge crossing. This is achieved by 2D Delaunay triangulation constrained by image borders and correspondent mesh CM_k borders. These new triangles are added to the SCM.

In the next section, we describe the wavelet analysis scheme applied on the base meshes in order to provide a multi-resolution scalable representation for each 3D model.

D. Wavelet decomposition

The goal of wavelet decomposition is to decorrelate geometric information so as to proceed to the first step towards compression. In addition, the multi-resolution aspect of this transform allows very efficient reconstruction and transmission, possibly in real-time [24].

Since we describe geometric deformations, first generation wavelets do not apply. Indeed, these parameterizations are defined over topological spaces (typically base meshes BM_k of Fig. 1) which are not linear spaces. Thus, wavelets themselves have to be defined according to the base domain, its subdivisions and geometric irregularities.

In the context of Subdivision Surfaces [20], wavelets can be defined starting from a low pass reconstruction filter P^j. This filter operates over a global topological subdivision consisting in facets quadrisections, similarly as interval dichotomies in the classical wavelet setting. Filter P^j transforms coefficients at level $j-1$ into a prediction at level j:

$$c^{j+1} = P^j c^j. \tag{1}$$

The resulting coefficients are an approximation, without adding any information, which coincides with the refinement operator in the case of Subdivision Surfaces. The wavelet setting can be seen as "completing" the representation by adding details through a high pass reconstruction filter Q^j. This filter has to satisfy an exact reconstruction criterion, which implies that matrix $(P^j Q^j)$ is invertible.

Scaling functions $(\phi_i^j)_i$ and wavelets $(\psi_i^j)_i$ are directly defined by these filters, so that the parameterization to transform can be expressed as

$$S = \sum_{j\geq 0} \sum_i d_i \psi_i^j + \sum_i c_i^0 \phi_i^0. \tag{2}$$

In our case, we use continuous piecewise linear wavelets, which implies that matrix P^j has the form $P = (I\ P')^t$ where I denotes identity and P' a canonical averaging matrix. As for matrix Q, it is chosen so that the resulting wavelets are stable and provide good compression. This is achieved by the requirement of vanishing moments through the lifting scheme [25].

For encoding depth maps, we start by defining a geometrical deformation as illustrated on Fig. 6. The transform is expressed as a scalar in terms of distance to the observer: the scalar function $\rho : MB_k -> \mathbf{R}$ maps a point x on the base mesh to the offset p between x and $M_{nm}^{i+1} \cap (C_k x)$.

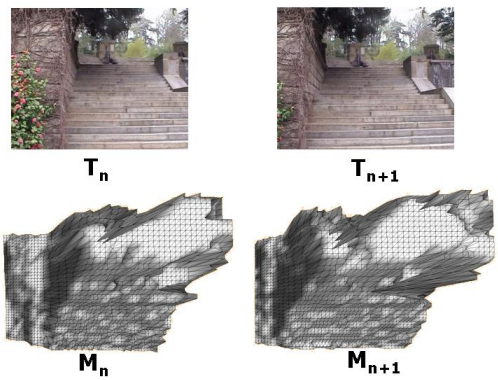

Fig. 5. Successive models for the *Thabor* sequence M_n(c), M_{n+1}(d) and associated texture image T_n(a), T_{n+1}(b) (lateral translation of the camera)

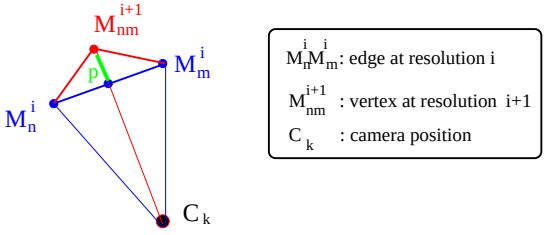

Fig. 6. Estimation of the depth to encode with wavelets

We then process the wavelet transform by applying $(P^j Q^j)^{-1}$ for every j:

$$\begin{pmatrix} c^j \\ d^j \end{pmatrix} = (P^j\ Q^j)^{-1} c^{j+1}. \tag{3}$$

The representation to encode is shown on Fig. 1. Fine models FM_i are represented by base meshes BM_k and wavelet coefficients r_i^j. Scale coefficients e_i^j expressing the geometry of base meshes are gathered and indexed by the SCM.

In classical decomposition all faces are subdivided at the same fixed level at the encoding stage . However all the faces of the mesh do not need to be subdivided at the same level depending on the size on the face and on the part of the scene they represent. Therefore we introduce an adaptive wavelet decomposition. The level a face is decomposed at is given by the size of the 3D face in order to gather two criteria; the depth gradient and the area of the 2D face of the image. Fig. 7 gives examples of meshes given by classical and adaptive decomposition for *Thabor* sequence.

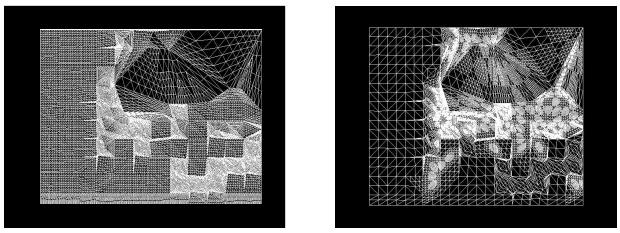

a (13765 vertices) b (10783 vertices)

Fig. 7. Example for sequence Thabor *: progressive meshes reconstructed with classical (a) and with adaptive (c) wavelet decomposition*

At this stage, we have obtained a set of multi-resolution meshes based on non-uniform triangulation, with corresponding vertices. This representation has several advantages, among which are:

- vertex positions can be adapted to scene contents;
- vertex to vertex correspondence between successive models is implicitly provided by the mesh structure and therefore does not need to be transmitted or estimated at the decoder side. It allows to smooth transitions between 3D models through implicit morphing using a simple linear interpolation between vertices.

This 3D representation for videos induces several media streams, such as topology (the connectivity of the single base mesh), geometry (wavelet coefficients and incremental model representation), and texture as well as camera parameters for each frame. Efficient coding of these streams is described in the next section.

V. Compression of the representation

A. Inter-relations between different media

A key observation is that the information streams to be transmitted are not independent and an efficient coding algorithm should take into account this redundancy for both compression rate and quality of the reconstructed sequence.

Here is the description of inter-relations occurring within 3D model-based coding that we use in our coder.

First of all camera positions can help the transmission of 3D models. Indeed, for each vertex of the non-uniform meshed model five coordinates have to be transmitted: three coordinates for vertex location (3D coordinates) and 2 for texture (2D coordinates). If the camera positions are known on the decoder side only three parameters instead of five are required. Indeed 2D texture coordinates can be retrieved by reprojecting 3D vertices M_j on camera position of the GOF key frame viewpoint. As the key frame is also the texture image, the coordinates of the resulting projection m_j are the texture coordinates for vertex M_j. These parameters can be the exact positions of 3D vertices M_j or texture coordinates m_j and the associated depth d_j if the 3D model is an elevation map. This is represented on Fig. 9 by the arrow (1).

Furthermore since 3D models represent overlapping parts of the scene, the related textures include redundant information. To exploit this redundant information compressing texture images using a classical scheme IPP where the first image is in Intra mode and the others are in Predicted mode is useful. Using 1D and 3D information predicted images can be estimated thanks to the reprojection of the precedent textured model onto associated camera (cf. Fig. 8). This is represented by the arrows (2) on Fig. 9.

a b

Fig. 8. *Thabor* sequence: Predicted images. Image 107 from original sequence (a) and associated predicted image (b).

In the same way, 3D models geometry share common information. This redundancy can be reduced by using an IPP scheme for 3D information. Predicted models are given by the common part of the precedent model. This is represented on Fig. 9 by the arrow (3). These inter-relations are summarized on Fig. 9. To taking into account those interrelations allows to dramatically reduce the bitrate [26].

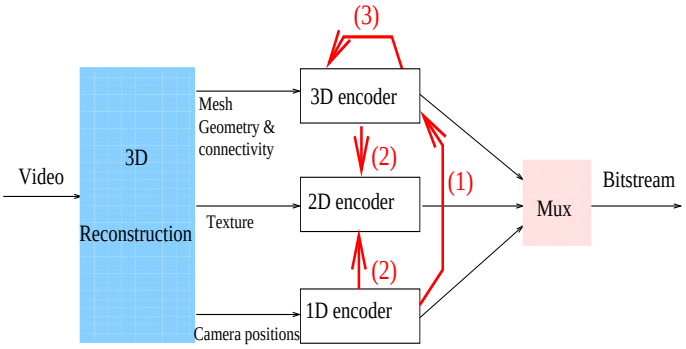

Fig. 9. Inter-relations between the media in 3D model-based coding

Depending on the envisioned applications, texture or geometry has to be favored. For instance, texture is very important in video broadcasting applications, because human vision is very sensitive to texture. In virtual reality applications (free viewpoint generation or addition of objects for example), 3D geometry has to be more accurate. With a unique stream instead of several ones we can update on the fly the rate

associated to each medium whose particular encoders are presented in the next section.

B. Camera encoding

Key frame camera positions are differentially encoded and intermediate camera positions are retrieved by linear interpolation between key positions:

$$C_c = \alpha * C_k + (1-\alpha) * C_{k+1} \text{ with } \alpha = \frac{\parallel t_{k+1} - t_c \parallel}{\parallel t_{k+1} - t_k \parallel}.$$

C. Texture encoding

An IPP scheme is used where predicted image $P(I_{k+1})$ are obtained by the reprojection of the precedent textured model on the current key position as described in Section V-A. Padding is used in areas where prediction does not apply (cf. Fig. 8:

$$P(K_{k+1}) = Pr({M_k}^i, T_k, C_{k+1}).$$

Fine granularity scalability for the texture images is allowed by EBCOT coder. The use of the IPP scheme hinder decoding scalability. Therefore we add a low bandwidth for texture transmission. At the coding stage, the image used in order to get the prediction is the precedent image, but decoded at very low bitrate. Refinements are transmitted in the error image.

D. Connectivity and 3D Geometry encoding

3D information encoding is based on the base mesh BM_k and a set of wavelet coefficients for refinements.

2D texture coordinates are not encoded, as explained in section V-A since they can be retrieved by reprojecting the 3D model on the related key position.

The base meshes are encoded using TS (Topological Surgery) encoder [10] for geometry and connectivity. We can rapidly identify vertices having a correspondent in the next model by re-projecting vertices of the current model on the key image of the next GOF. In this way, we retrieve the common information between two models at the decoding stage without transmitting additional information. The global indexing system introduced in Section IV helps to implicitly encode correspondences between successive base meshes. In order to avoid numerical errors a stage of robust selection of base mesh vertices is added to Harris corner selection.

After the wavelet transform, we get some sets of wavelet coefficients $(r_i^j)_i^j$ with low first order entropy. This representation is then binarized using a zero-tree algorithm suited to the geometric setting [21][27]. To this end, a special hierarchy is setup on the mesh, ordering vertices instead of facets. The SPIHT algorithm can be applied directly onto this hierarchy, similarly to the 2D case. The use of this adaptation of the SPIHT zero-tree encoder adds bitplane scalability.

Note that the SPIHT algorithm does not contain any entropy coding stage. It is possible to take advantage of such a coding in a post-process, but this may not be desirable in the case of adaptive decoding or bitstream degradation, since it makes real-time decoding slower.

VI. Results and discussion

We show results on two sequences, illustrating the compression rates reached by comparison to Galpins and H264 encoders at low and very low bitrates on both constrained and free navigation.

For the wavelet decomposition we use the classical midpoint bi-orthogonal analysis performing a sub-sampling [25].

A. Visual quality and PSNR

While PSNR is appropriate for measuring block based errors, it has however, little meaning when it comes to geometric distortion. Global distortion on reconstructed images is produced both by texture (texture image compression artefacts) and geometric distortions (from 3D model estimation errors and depth compression artefacts). Geometric distortion greatly decreases PSNR when it may have little impact on visual quality. A demonstrative example is the geometric distortion defined by a one pixel translation.

This is shown by comparing visual quality and PSNR of texture images and reconstructed images, as in Fig. 10. The texture image PSNR is the PSNR obtained with texture distortion alone, and without geometric distortion. It is dramatically much larger than the eventual PSNR value on reconstructed image, but visual quality is equivalent for both images.

Thus, low PSNR values of reconstructed images are essentially due to geometric distortion, but they do not reflect visual quality, which is more related to texture accuracy.

(a) 29.6603 (b) 26.2669

Fig. 10. *Thabor* sequence: texture image (a) and reconstructed image (b). While its PSNR is much lower the visual quality of the reconstructed image is similar to the texture image visual quality.

We thus show PSNR values in an informative way and rather rely on visual assessment of the reconstructed images, in particular in the case of free view point generation for which PSNR has little meaning.

B. Compression results

We show compression results for a sequence of 110 frames of the *Thabor* sequence for low and very low bitrates on Fig. 11 and 12. No comparison can be made with H264 if such a low rate cannot be reached at 25Hz.

In Galpin's method depth maps were encoded as an image with EBCOT. The number of vertices in the uniform mesh is then reduced to be competitive with the rate achieved by our progressive coder (15kb for 2400 vertices against 22kb for 1600 vertices for Galpin's coding for the stairs sequence). This profits allows to allocate more bitrate for texture information in order to better preserve texture details (as shown on Fig. 12 on the wall on the right or in the background on the image).

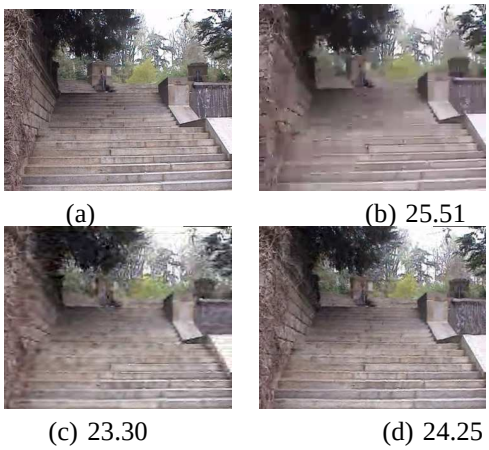

Fig. 11. *Thabor* sequence: Image 127 from original sequence (CIF, 25Hz) (a) and reconstructed images at 125kb/s with H264 coder (b), with Galpin coder (c) and with our coder (d)

Fig. 12. *Thabor* sequence: Reconstructed images 71 at 30kb/s with Galpin coder (a) and with our coder (b)

Since texture information is prominent over geometry for low bitrates, this profit is particularly useful in order to achieve very low bitrate.

C. Scalability Results

Here we show some results of the scalability obtained with our coder. We show PSNR values even if it does not allow the evaluation of the quality of the reconstructed sequence, because of geometric distortion.

The table of the Fig. 13 shows the number of vertices and the associated rate depending on the level of the wavelet decomposition. Fig. 14 shows reconstructed images associated with these levels of decomposition. The size of the binary representation increases with the wavelet decomposition level, and so does the quality of the reconstructed images. This is particularly visible on the steps of the stairs. For this sequence the choice of level 2 seems to be a good rate / distortion trade-off.

Level	Number of Vertices	size (bits)
0	148	7744
1	565	10869
2	2185	17155
3	8736	29806

Fig. 13. Number of vertices and associated rate function of the level of the wavelet decomposition

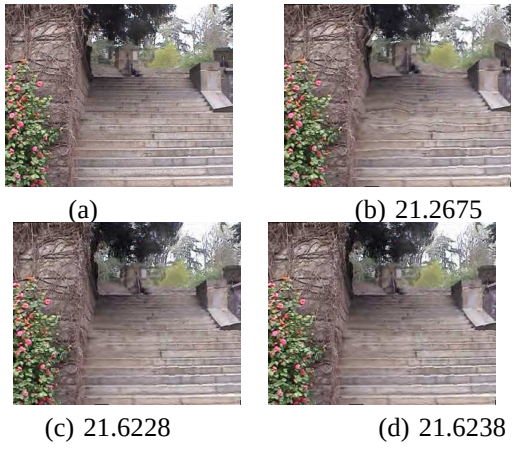

Fig. 14. *Thabor* sequence: spatial scalability Image 71 from the original sequence (CIF, 25Hz) (a) and reconstructed images at 125kb/s at different level of wavelet decomposition 0 (b), 2 (c) and 3 (d).

D. Virtual navigation results

Including inter-relations into the coder not only dramatically decreases compression rates but it also increases the visual quality of the reconstructed sequence by linking up different models together.

Fig. 15 shows successive images around a transition between two GOFs, the last of the preceding GOF and the first of the following. One can see the discontinuity between two successive frames of the video on these images with the right-hand edge blank due to missing information for appearing areas. Fig. 15 shows also the same images reconstructed with our method. The artefacts are greatly reduced by the morphing enabled by model vertex matching.

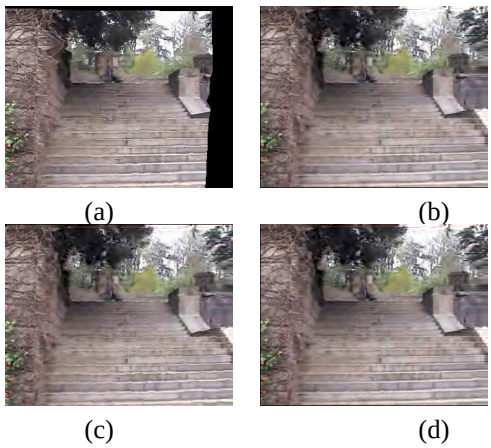

Fig. 15. *Thabor* sequence: Reconstruction of original path around a transition between two successive models. Successive reconstructed images without post-treatment (no morphing nos fading) (a) and (b). Successive reconstructed images with our coder (c) and (d).

Galpin 3D fading [17] allows to reduce artefacts near model transitions but it also produces ghost effects on images of the middle of the GOF and on images associated to free viewpoints. The implicit morphing strongly contributes to the visual quality of the scene, avoiding these ghost effects while smoothing transitions between models.

Fig. 16 shows reconstruction results during free navigation,

i.e. when the viewer is not restricted to the camera path defined during capture. In a similar way results on the original path visual quality of reconstructed images is increased by eliminating artefacts of ghost effects even though some geometric distortions are visible near the upper image border, due to non uniform triangulation.

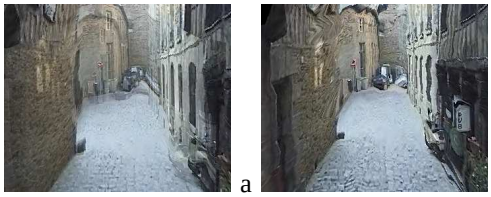
a b

Fig. 16. Street sequence: Reconstruction on virtual path with Galpin (a) and with proposed method (b).

Our algorithm is however limited by occlusions and by 3D informations and camera parameters precision. Our approach do not require an accurate geometry and therefore the models can not be used to generate a free viewpoint far from the original camera.

VII. Conclusions and future work

We have presented a new model-based coding scheme for static video with fine-grain scalability, allowing content adaptation over a very wide spectrum of terminals and networks. This scheme takes advantage of specific video content, i.e. a fixed scene acquired with a moving camera, to build a 3D representation which allows better performances and advanced functionalities. In particular, 3D can be streamed adaptively in applications of free navigation over networks. The coder, showing better compression results and finer scalability than previous schemes, exploits all the power of second generation wavelets and implicit morphing thanks to the design of a connectivity mesh gathering each GOF connectivity information.

To further improve this scheme it would be interesting to express the temporal increments in a wavelet basis themselves. Furthermore, reconstructed images have shown the need for a suitable error metric for reconstructed images taking into account the geometric distortion to meet visual quality measure. Finally whereas encoding/decoding the representation can be done on-line, non-linear optmizations for disparity estimation or bundle adjustment harm complexity of the 3D extraction algorithm. It could be interesting to try new graphics processors to accelerate treatments to reach real-time applications such as video-conferencing.

References

[1] H. Schwarz and T. Wiegrand, "The emerging jvt/h.26l video coding standard," in *Proc. IBC, Amsterdam, 2002*, 2002.

[2] F. Preteux and M. Malciu, "Model-based head tracking and 3d pose estimation," in *Visual Conference on Image Processing*, 1998, pp. 94–110.

[3] B. Girod and al., "3d image models and compression - synthetic hybrid or natural fit?" in *Proc. ICIP*, Oct. 1999.

[4] R. Koch, M. Pollefeys, and L. V. Gool, "Realistic surface reconstruction of 3d scenes from uncalibrated image sequence," *Journal of Visualization and Computer Animation*, vol. 11, pp. 115–127, 2000.

[5] M. Pollefeys, M. Vergauwen, F. Verbiest, K. Cornelis, and L. V. Gool, "From image sequences to 3d models," in *Third International Workshop on Automatic Extraction of Man-made Objects from Aerial and Space Images*, 2001.

[6] A. Zisserman, A. Fitzgibbon, and G. Cross, "Vhs to vrml: 3d graphical models from video sequences," in *IEEE International Conference on Multimedia Computing and System*, vol. 1, June 1999, pp. 51–57.

[7] D. Nister, "Reconstruction from uncalibrated sequences with a hierarchy of trifocal tensors," in *Proc. of the 5th European Conference on Computer Vision ECCV'2000, Dublin, Ireland*, 2000.

[8] K. Cornelis, M. Pollefeys, M. Vergauwen, and L. V. Gool, "Augmented reality using uncalibrated video sequences," in *Proc. Second Workshop on Structure fromMultiple Images of Large Scale Environments*, 2000.

[9] P. Alliez and C. Gotsman, "Recent advances in compression of 3d meshes," in *Proc. of the Symposium on Multiresolution in Geometric Modeling*, 2003.

[10] G. Taubin and J. Rossignac, "Geometric compression through topological surgery," *ACM Trans. Graph.*, vol. 17, no. 2, pp. 84–115, 1998.

[11] J. Rossignac, "Edgebreaker: Connectivity compression for triangle meshes," *IEEE Transactions on Visualization and Computer Graphics*, pp. 47–61, 1999.

[12] I. JTC1/SC29/WG11, "Applications and requirements for 3dav," 2003.

[13] E. Lamboray, S. Würmlin, and M. Gross, "Real-time streaming of point-based 3d video," in *Proc. of the IEEE Virtual Reality conference*, 2004, pp. 91–98.

[14] M. Magnor, P. Ramanathan, and B.Girod, "Multi-view coding for image based rendering using 3d scene geometry," *IEEE Transactions on Circuits and Systems for Video Technology*, 2003.

[15] P. Ramanathan and B. Girod, "Random access for compressed light fields using multiple representations," in *Proc. of the Conference on Computer Vision and Pattern Recognition*, 2004.

[16] F. Galpin, R. Balter, L. Morin, and K. Deguchi, "3d models coding and morphing for efficient video compression," in *Proc. of the Conference on Computer Vision and Pattern Recognition*, 2004.

[17] F. Galpin and L. Morin, "Sliding adjustment for 3d video representation," *Eurasip Journal ASP, special issue on Signal Processing for 3D Imaging and Virtual reality*, 2002.

[18] B. L. Guen, R. Balter, L. Morin, and P. Alliez, "Morphing de modeles 3d estimes," in *Journes d'tudes et d'changes CORESA'2004*, mai 2004.

[19] I. Daubechies, *Ten lectures on wavelets*, society for industrial and applied mathematics ed. Philadelphia, PA: CBMS-NSF regional conf. series in appl. math., 1992, vol. 61.

[20] M. Lounsbery, T. D. DeRose, and J. Warren, "Multiresolution analysis for surfaces of arbitrary topological type," *ACM Transactions on Graphics*, vol. 16, no. 1, pp. 34–73, Jan. 1997, iSSN 0730-0301.

[21] A. Khodakovsky, P. Schroder, and W. Sweldens, "Progressive geometry compression," in *SIGGRAPH 2000 Conference Proceedings*, 2000.

[22] S. Pateux, G. Marquant, and D. Chavira-Martinez, "Object mosaicking via meshes and crack-lines technique. application to low bit-rate video coding," in *Proc. of Picture Coding Symposium*, 2001.

[23] C. Harris and M. Stephens, "A combined corner and edge detector," in *Proc. 4th Alvey Vision Conf.*, 1988.

[24] P. Gioia, O. Aubault, and C. Bouville, "Real-time reconstruction of wavelet encoded meshes for view-dependent transmission and visualization," *IEEE Transactions on CSVT*, 2004.

[25] P. Schroder and W. Sweldens, "Spherical wavelets : Efficiently representing functions on the sphere," in *Siggraph 95*, 1995, pp. 161–172.

[26] R. Balter, P. Gioia, L. Morin, and F. Galpin, "Scalable and efficient coding of 3d model extracted from a video," in *3DPTV, september*, 2004.

[27] A. Said and W. A. Pearlman, "A new fast and efficient image codec based on set partitioning in hierarchical trees," *IEEE Transactions on Circuits and Systems for Video Technology*, 1996.